Inorg. Chem. **2002**, *41*, 6071–6079

Application of Time-Resolved Infrared Spectroscopy to Electronic Structure in Metal-to-Ligand Charge-Transfer Excited States

Dana M. Dattelbaum,[†,‡] Kristin M. Omberg,[‡] Jon R. Schoonover,*[,‡] Richard L. Martin,[§] and Thomas J. Meyer*[,∥]

Department of Chemistry, University of North Carolina, Chapel Hill, North Carolina 27599-3290, Materials Science and Technology Division, Mail Stop E549, and Theoretical Division, Mail Stop B268, Los Alamos National Laboratory, Los Alamos, New Mexico 87545

Received June 13, 2002

Infrared data in the ν(CO) region (1800–2150 cm^{-1}, in acetonitrile at 298 K) are reported for the ground ($\bar{\nu}_{gs}$) and polypyridyl-based, metal-to-ligand charge-transfer (MLCT) excited ($\bar{\nu}_{es}$) states of *cis*-[Os(pp)$_2$(CO)(L)]$^{n+}$ (pp = 1,-10-phenanthroline (phen) or 2,2′-bipyridine (bpy); L = PPh_3, CH_3CN, pyridine, Cl, or H) and *fac*-[Re(pp)(CO)$_3$(4-Etpy)]$^+$ (pp = phen, bpy, 4,4′-$(CH_3)_2$bpy, 4,4′-$(CH_3O)_2$bpy, or 4,4′-$(CO_2Et)_2$bpy; 4-Etpy = 4-ethylpyridine). Systematic variations in $\bar{\nu}_{gs}$, $\bar{\nu}_{es}$, and $\Delta\bar{\nu}$ ($\Delta\bar{\nu} = \bar{\nu}_{es} - \bar{\nu}_{gs}$) are observed with the excited-to-ground-state energy gap (E_0) derived by a Franck–Condon analysis of emission spectra. These variations can be explained qualitatively by invoking a series of electronic interactions. Variations in dπ(M)–π*(CO) back-bonding are important in the ground state. In the excited state, the important interactions are (1) loss of back-bonding and σ(M–CO) bond polarization, (2) π*(pp•$^-$)–π*(CO) mixing, which provides the orbital basis for mixing π*(CO)- and π*(4,4′-X$_2$bpy)-based MLCT excited states, and (3) dπ(M)–π(pp) mixing, which provides the orbital basis for mixing $\pi\pi$*- and π*(4,4′-X$_2$-bpy•$^-$)-based MLCT states. The results of density functional theory (DFT) calculations on the ground and excited states of *fac*-[Re^{I}(bpy)(CO)$_3$(4-Etpy)]$^+$ provide assignments for the ν(CO) modes in the MLCT excited state. They also support the importance of π*(4,4′-X$_2$bpy•$^-$)–π*(CO) mixing, provide an explanation for the relative intensities of the A′(2) and A″ excited-state bands, and provide an explanation for the large excited-to-ground-state ν(CO) shift for the A′(2) mode and its relative insensitivity to variations in X.

Introduction

Time-resolved infrared (TRIR) spectroscopy has been successfully applied to a number of issues related to excited-state molecular and electronic structure in polypyridyl complexes containing carbonyl ligands.[1−9] The ν(CO) vibrations have high oscillator strengths, and their energies are sensitive to changes in electronic structure at the metal. The magnitudes of shifts in the ν(CO) band energies between the ground and excited states depend on the electronic origin of the excited state. In polypyridyl-based, metal-to-ligand charge-transfer (MLCT) excited states, ν(CO) increases 50−100 cm^{-1} compared to that in the ground state. This is due to the change in electronic configuration from dπ^6 to d$\pi^5\pi^{*1}$, eq 1 (bpy is 2,2′-bipyridine; 4-Etpy is 4-ethylpyridine), which decreases electron density at the metal and, with

$$\underset{^1d\pi^6}{[(bpy)Re^{I}(CO)_3(4\text{-}Etpy)]^+} \xrightarrow{h\nu} \underset{d\pi^5\pi^{*1}}{[(bpy^{\bullet-})Re^{II}(CO)_3(4\text{-}Etpy)]^+} \quad (1)$$

* Authors to whom correspondence should be addressed. E-mail: schoons@lanl.gov (J.R.S.); tjmeyer@lanl.gov (T.J.M.).
† University of North Carolina.
‡ Materials Science and Technology Division, Los Alamos National Laboratory.
§ Theoretical Division, Los Alamos National Laboratory.
∥ Associate Director for Strategic Research, Mail Stop A127, Los Alamos National Laboratory.
⊥ Contribution No. 3290.

(1) Abbott, L. C.; Arnold, C. J.; Ye, T.-Q.; Gordon, K. C.; Perutz, R. N.; Hester, R. E.; Moore, J. N. *J. Phys. Chem. A* **1998**, *102*, 1252−1260.
(2) Schoonover, J. R.; Bignozzi, C. A.; Meyer, T. J. *Coord. Chem. Rev.* **1997**, *165*, 239−266.
(3) Schoonover, J. R.; Strouse, G. F.; Dyer, R. B.; Bates, W. D.; Chen, P.; Meyer, T. J. *Inorg. Chem.* **1996**, *35*, 273−274.
(4) Stufkens, D. J.; Vlcek, A., Jr. *The Spectrum* **1996**, *9*, 2−7.
(5) Schoonover, J. R.; Strouse, G. F.; Omberg, K. M.; Dyer, R. B. *Comments Inorg. Chem.* **1996**, *18*, 165.
(6) Rossenaar, B. D.; George, M. W.; Johnson, F. P. A.; Stufkens, D. J.; Turner, J. J.; Vlcek, A., Jr. *J. Am. Chem. Soc.* **1995**, *117*, 11582−11582.
(7) Turner, J. J.; George, M. W.; Johnson, F. P. A.; Westwell, J. R. *Coord. Chem. Rev.* **1993**, *93*, 101.
(8) Schoonover, J. R.; Gordon, K. C.; Argazzi, R.; Woodruff, W. H.; Peterson, K. A.; Bignozzi, C. A.; Dyer, R. B.; Meyer, T. J. *J. Am. Chem. Soc.* **1993**, *115*, 10996−10997.
(9) Glyn, P.; George, M. W.; Hodges, P. M.; Turner, J. J. *J. Chem. Soc., Chem. Commun.* **1989**, 1655.

10.1021/ic020400i CCC: $22.00
Published on Web 10/25/2002

it, $d\pi(Re)-\pi^*(CO)$ back-bonding. In $d\pi^6$ polypyridyl complexes of Ru(II), Os(II), and Re(I) light absorption is dominated by MLCT excitation to states that are largely singlet in character. Emission comes from a manifold of Boltzmann-populated, low-lying states, which are largely triplet in character.[10−12] These states have a common $d\pi^5\pi^{*1}$ orbital origin.

TRIR has also been used to identify the lowest-lying excited states of d^6 metal complexes by fingerprinting,[2−9] to establish localization or delocalization in mixed-valence[1,13] and MLCT excited state(s),[13,14] and to demonstrate polarization of the excited electron in asymmetrical acceptor ligands such as 4-CO_2Et-4′-CH_3-2,2′-bipyridine and 4-$CONEt_2$-4′-CH_3-2,2′-bipyridine.[15]

We report here the application of TRIR in the ν(CO) region, combined with synthetic manipulation, emission measurements, and density functional calculations to explore MLCT excited-state electronic structure in two series of complexes with well-characterized MLCT excited states.[16,17] In *cis*-$[Os(pp)_2(CO)(L)]^{n+}$ (pp = 1,10-phenanthroline (phen) or 2,2′-bipyridine (bpy); L = PPh_3, CH_3CN, pyridine, Cl, or H) variations in the ancillary ligand L lead to systematic variations in the MLCT excited-to-ground-state energy gap. Changes in electronic structure at Os are monitored by using ν(CO) as a spectator vibration.

In the second series, *fac*-$[Re(pp)(CO)_3(4\text{-Etpy})]^+$ (pp = phen, bpy, 4,4′-$(CH_3)_2$bpy, 4,4′-$(CH_3O)_2$bpy, or 4,4′-$(CO_2Et)_2$bpy; 4-Etpy = 4-ethylpyridine), the energy gap is varied by varying the 4,4′-substituents on the acceptor ligand, and the three ν(CO)-based normal modes are used to probe electronic structure. The polypyridyl ligands used in this study are illustrated below:

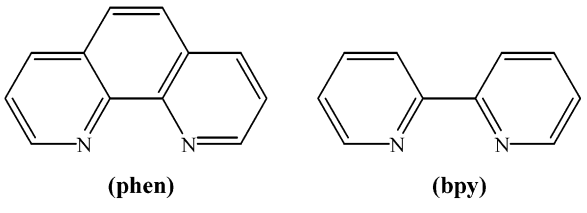

Experimental Section

Materials. Acetonitrile was obtained from Aldrich and used without further purification. *cis*-$[Os(bpy)_2(CO)(PPh_3)](PF_6)_2$, *cis*-$[Os(bpy)_2(CO)(CH_3CN)](PF_6)_2$, *cis*-$[Os(bpy)_2(CO)(py)](PF_6)_2$, *cis*-$[Os(bpy)_2(CO)Cl](PF_6)$, *cis*-$[Os(phen)_2(CO)Cl](PF_6)$, and *cis*-$[Os(phen)_2(CO)H](PF_6)$ (py is pyridine) were prepared according to literature procedures.[18] *fac*-$[Re(phen)(CO)_3(4\text{-Etpy})](PF_6)$, *fac*-$[Re(4,4'\text{-}(CH_3)_2bpy)(CO)_3(4\text{-Etpy})](PF_6)$, *fac*-$[Re(4,4'\text{-}(CH_3O)_2bpy)(CO)_3(4\text{-Etpy})](PF_6)$, *fac*-$[Re(bpy)(CO)_3(4\text{-Etpy})](PF_6)$, and *fac*-$[Re(4,4'\text{-}(CO_2Et)_2bpy)(CO)_3(4\text{-Etpy})](PF_6)$ were also prepared according to literature procedures.[16,19] Tetra-*n*-butylammonium hexafluorophosphate (TBAH) was obtained from Aldrich and recrystallized twice from ethanol.

Emission Spectra. Corrected emission spectra were recorded on a Spex Fluorolog-2 emission spectrometer equipped with a 450 W Xe lamp and cooled 10-stage Hammamatsu R928 or R664 photomultipliers. The response from the photomultipliers was corrected with a calibration curve generated with 1.0 mm slits by using a NIST-calibrated standard lamp (Optronics Laboratories, Inc. model 220M) controlled with a precision current source at 6.50 W (Optronics Laboratories, Inc. model 65). The manufacturer's recommendations regarding lamp geometry were followed. All spectra were acquired in acetonitrile solution at room temperature in 1 cm path length quartz cells (OD < 0.05) by using right-angle observation of the emitted light.

Electrochemical Measurements. Electrochemical measurements were conducted under nitrogen in a drybox by using an EG&G PAR model 273 potentiostat. Cyclic voltammetry measurements utilized a standard three-compartment cell with platinum working and counter electrodes and a $Ag/AgNO_3$ (0.01 M $AgNO_3$/0.1 M TBAH in acetonitrile) reference electrode, which was regularly calibrated with a saturated sodium chloride/calomel electrode (SSCE). All potentials are reported versus SSCE.

Infrared Spectra. Infrared measurements utilized a BioRad FTS 60A/896 step-scan interferometer with an external MCT detector as previously described.[13] A recent upgrade of this instrument utilizes fast data-processing techniques. In this arrangement, the IR signal from the detector was amplified and processed by a BioRad Fast TRS board installed in a Pentium PC. This board also controlled the mirror movement, which was operated at 10 Hz.

Samples were excited at 355 nm by using the third harmonic of a Nd:YAG laser (Spectra Physics GCR-11, 7 ns pulse width, operated at 10 Hz). Individual points on the interferogram were collected by the interferometer software every 200 ns after the laser pulse for 1 μs. The data were organized into individual interferograms representing the interferogram at every 200 ns point, and then Fourier transformed into spectra. The spectra were averaged between the laser pulse and 800 ns to give the final TRIR spectra. The ground- and excited-state spectra shown are an average of 64 scans.

Samples for TRIR Studies. All IR spectra were measured in acetonitrile, in a 1 mm path length sealed CaF_2 cell. Sample concentrations were adjusted to give an absorbance of ~0.7 for the ν(CO) bands. The sample cell and sample solutions were deoxygenated by sparging with argon for 15 min and the solutions transferred to the cell under an inert atmosphere. The spectra were acquired in 2 blocks of 32 to prevent sample decomposition and averaged to give the final spectra.

(10) Kober, E. M.; Meyer, T. J. *Inorg. Chem.* **1984**, *23*, 3877−3886.
(11) Crosby, G. A. *Acc. Chem. Res.* **1975**, *8*, 231−238.
(12) Striplin, D. R.; Crosby, G. A. *Chem. Phys. Lett.* **1994**, *221*, 426−430.
(13) Omberg, K. M.; Schoonover, J. R.; Treadway, J. A.; Leasure, R. M.; Dyer, R. B.; Meyer, T. J. *J. Am. Chem. Soc.* **1997**, *119*, 7013−7018.
(14) Omberg, K. M.; Schoonover, J. R.; Meyer, T. J. *J. Phys. Chem.* **1997**, *101*, 9531.
(15) Chen, P.; Omberg, K. M.; Kavaliunas, D. A.; Treadway, J. A.; Palmer, R. A.; Meyer, T. J. *Inorg. Chem.* **1997**, *36*, 954−955.
(16) Worl, L. A.; Duesing, R.; Chen, P.; Della Ciana, L.; Meyer, T. J. *J. Chem. Soc., Dalton Trans.* **1991**, 849−858.
(17) Kober, E. M.; Caspar, J. V.; Lumpkin, R. S.; Meyer, T. J. *J. Phys. Chem.* **1986**, *90*, 3722−3734.
(18) Sullivan, B. P.; Caspar, J. V.; Johnson, S. R.; Meyer, T. J. *Organometallics* **1984**, *3*, 1241−1251.
(19) Chen, P.; Duesing, R.; Graff, D. K.; Meyer, T. J. *J. Phys. Chem.* **1991**, *95*, 5850−5858.

Table 1. Ground-State ($\bar{\nu}_{gs}$) and Excited-State ($\bar{\nu}_{Es}$) Infrared Band Energies (± 2 cm^{-1}) and Shifts ($\Delta\bar{\nu} = \bar{\nu}_{es} - \bar{\nu}_{gs}$), Energy Gaps ($E_0$), and $E_{1/2}$ Values for *cis*-[Os(pp)$_2$((co)(L)]$^{n+}$ in Acetonitrile at 298 K

complex[a]	$\Delta\bar{\nu}$ (cm^{-1})	$\bar{\nu}_{gs}$ (cm^{-1})	$\bar{\nu}_{es}$ (cm^{-1})	E_0[b] (cm^{-1})	$E_{1/2}(Os^{III/II})$[c] (V)	$E_{1/2}(bpy^{0/-})$[c] (V)
cis-[Os(bpy)$_2$(CO)(PPh$_3$)]$^{2+}$	42	1975	2017	19200	1.98	−1.09
cis-[Os(bpy)$_2$(CO)(CH$_3$CN)]$^{2+}$	68	1979	2047	18400	1.80	−1.14
cis-[Os(bpy)$_2$(CO)(py)]$^{2+}$	69	1972	2041	17300	1.67	−1.15
cis-[Os(bpy)$_2$(CO)Cl]$^{+}$	74	1948	2022	14600	1.18	−1.29
cis-[Os(phen)$_2$(CO)Cl]$^{+}$	75	1950	2025	14800	1.14	−1.24
cis-[Os(phen)$_2$(CO)H]$^{+}$	76	1911	1987	14000[d]	0.90	−1.43

[a] As PF_6^- salts. [b] From Table 2. [c] Vs SSCE. [d] The emission was too low in energy to fit accurately. The value cited was calculated from the differences between E_{em} values in Table 2.

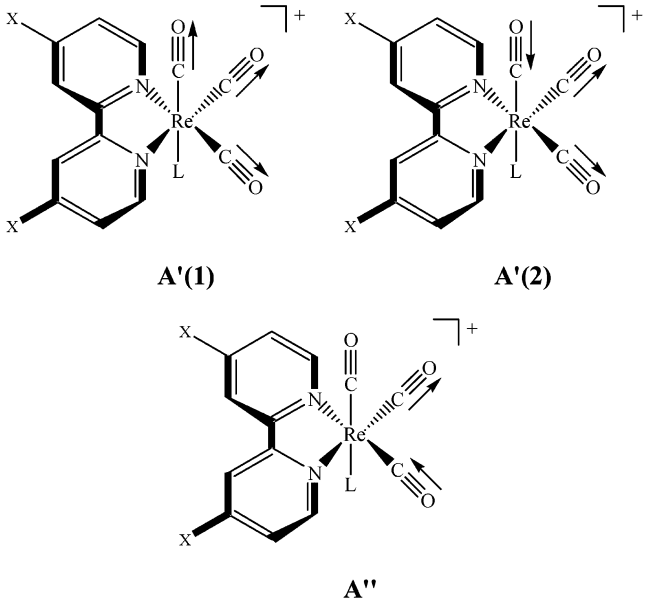

Figure 1. Local mode contributions to the A′(1), A′(2), and A″ normal modes in [Re^{II}(pp•$^-$)(CO)$_3$(4-Etpy)]$^{+}$*.

Density Functional Theory (DFT) Calculations. The hybrid B3LYP DFT approximation,[20] as implemented in the G98 package,[21] was used to determine the geometries and associated frequencies of the lowest singlet and triplet states. The metal centers were described by the "small core" LANL2 relativistic effective core potential[22] and the associated basis set. The latter was completely uncontracted, except that, for the resulting two primitive p functions with exponents 0.4960 and 0.4644, only the latter was retained to avoid linear dependency. This results in a (5s5p3d) basis for the metal. The 6-31G* basis set was used for the ligand atoms.

Results

***cis*-[Os(pp)$_2$(CO)(L)]$^{n+}$.** Ground- and excited-state ν(CO) band energies for *cis*-[Os(pp)$_2$(CO)(L)]$^{n+}$ are listed in Table 1. Also listed are the excited-state shifts ($\Delta\bar{\nu} = \bar{\nu}_{es} - \bar{\nu}_{gs}$), emission maxima, and $E_{1/2}$ values for the first ligand-based reduction and metal-based oxidation vs SSCE in acetonitrile at 298 K. Representative ground-state and TRIR spectra for *cis*-[Os(bpy)$_2$(CO)(CH$_3$CN)]$^{2+}$ are shown in Figure 2.

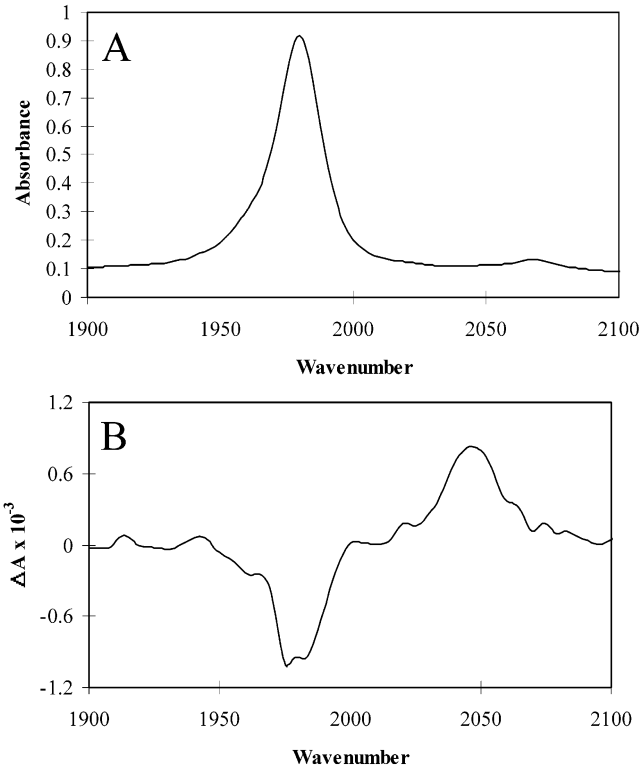

Figure 2. Ground-state (A) and TRIR (B) spectra of *cis*-[Os(bpy)$_2$(CO)(CH$_3$CN)]$^{2+}$ between 1900 and 2100 cm^{-1} at 298 K in CH$_3$CN.

Emission spectral fitting parameters E_0, S, and $\Delta\bar{\nu}_{1/2}$, derived by using a single-mode, Franck−Condon analysis of emission spectral profiles, as previously described,[17,23] in acetonitrile at 298 K, are listed in Table 2. E_0 is the maximum for the $\upsilon = 0 \rightarrow \upsilon' = 0$ vibronic component, $\Delta\bar{\nu}_{1/2}$ is the bandwidth at half-height, and S is the electron-vibrational coupling constant or Huang−Rhys factor. The quantum spacing, $\hbar\omega$, was fixed at 1300 cm^{-1} in the fits. This value is consistent with a value estimated from an analysis of resonance Raman spectral profiles, and represents the intensity-weighted average of 11 symmetric, in-plane, polypyridyl-based ring-stretching modes which appear as resonantly enhanced, Raman-active bands between 1000 and 1600 cm^{-1}.[17,24,25]

(20) Becke, A. D. *J. Chem. Phys.* **1993**, *98*, 1372.
(21) Frisch, M. J.; Trucks, G. W.; Schlegel, H. B.; Scuseria, G. E.; Robb, M. A.; Cheeseman, J. R.; Zakrzewshi, V. G.; Montgomery, J. A., Jr.; Stratmann, R. E.; Burant, J. C.; Dapprich, S.; Millam, J. M.; Daniels, A. D.; Kudin, K. N.; Strain, M. C.; Farkas, O.; Tomasi, J.; Barone, V.; Cossi, M.; Cammi, R.; Mennucci, B.; Pomelli, C.; Adamo, C.; Clifford, S.; Ochterski, J.; Petersson, G. A.; Ayala, P. Y.; Cui, Q.; Morokuma, K.; Malick, D. K.; Rabuck, A. D.; Raghavachari, K.; Foresman, J. B.; Cioslowski, J.; Ortiz, J. V.; Baboul, A. G.; Stefanov, B. B.; Liu, G.; Liashenko, A.; Piskorz, P.; Komaroni, I.; Gomparts, R.; Martin, R. L.; Fox, D. J.; Keith, T.; Al-Laham, M. A.; Peng, C. Y.; Wong, M. W.; Andres, J. L.; Gonzolez, C.; Head-Gordon, M.; Replogle, E. S.; Pople, J. A., Gaussian Inc., Pittsburgh, PA, 1998.
(22) Hay, P. J.; Wadt, W. R. *J. Chem. Phys.* **1995**, *82*, 299.
(23) Claude, J. P.; Meyer, T. J. *J. Phys. Chem.* **1995**, *99*, 51−54.
(24) Myers, A. B. *Chem. Rev.* **1996**, *96*, 911.
(25) Strommen, D. P.; Mallick, P. K.; Danzer, G. D.; Lumpkin, R. S.; Kincaid, J. R. *J. Phys. Chem.* **1990**, *94*, 1357.

Table 2. Emission Spectral Fitting Parameters for *cis*-$[Os(pp)_2(CO)(L)]^{n+}$ in Acetonitrile at 298 K[a]

complex[b]	$\Delta\bar{\nu}$[c] (cm^{-1})	E_{em} (cm^{-1})	E_0 (cm^{-1})	S	$\Delta\bar{\nu}_{1/2}$ (cm^{-1})
cis-$[Os(bpy)_2(CO)(PPh_3)]^{2+}$	42	18000	19200	1.7	2017
cis-$[Os(bpy)_2(CO)(CH_3CN)]^{2+}$	68	17800	18400	1.4	2058
cis-$[Os(bpy)_2(CO)(py)]^{2+}$	69	16800	17300	1.2	2070
cis-$[Os(bpy)_2(CO)Cl]^{+}$	74	14200	14600	1.2	2300
cis-$[Os(phen)_2(CO)Cl]^{+}$	75	14300	14800	1.2	2160
cis-$[Os(phen)_2(CO)H]^{+}$	76	13500	14000[d]		

[a] $\hbar\omega$ was fixed at 1300 cm^{-1}. [b] As PF_6^- salts. [c] From Table 1. [d] The emission was too low in energy to fit accurately. The value cited was calculated from the differences between E_{em} values.

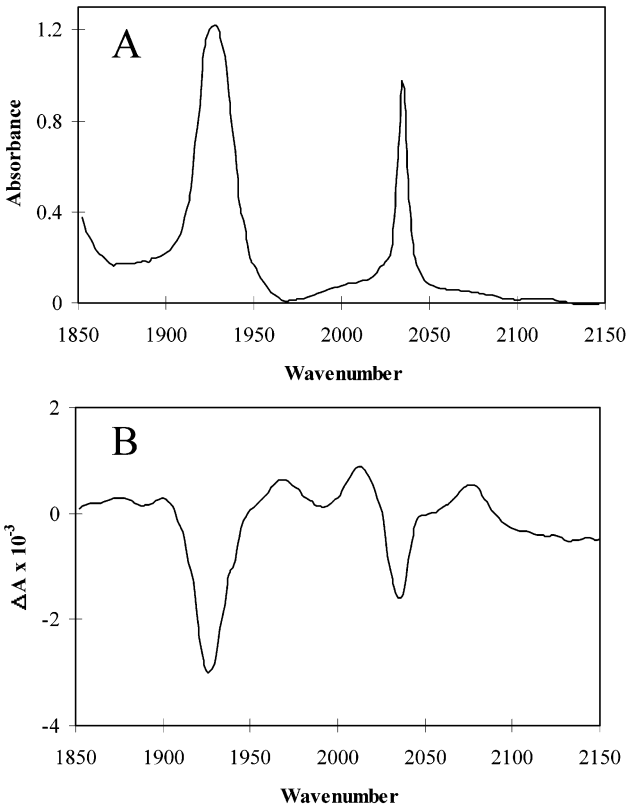

Figure 3. Ground-state (A) and TRIR (B) spectra of *fac*-$[Re(bpy)(CO)_3(4\text{-}Etpy)]^+$ between 1850 and 2150 cm^{-1} at 298 K in CH_3CN.

***fac*-[Re(pp)(CO)$_3$(4-Etpy)]$^+$.** Ground- and excited-state ν(CO) band energies for the series *fac*-$[Re(pp)(CO)_3(4\text{-}Etpy)]^+$ are listed in Table 3. Also listed are the excited-state shifts ($\Delta\bar{\nu} = \bar{\nu}_{es} - \bar{\nu}_{gs}$), emission maxima, and $E_{1/2}$ values for the first reduction and oxidation. Representative ground-state and TRIR spectra, for *fac*-$[Re(bpy)(CO)_3(4\text{-}Etpy)]^+$, are shown in Figure 3. Emission spectral fitting parameters in acetonitrile at 298 K are listed in Table 4. For these fits, $\hbar\omega$ was fixed at 1450 cm^{-1}. This value is higher for the Re complexes due to a contribution to the average mode from the high-energy, totally symmetric CO stretch at ~2030−2040 cm^{-1} (Table 3).[19,23]

DFT Calculations. Density functional calculations were performed on $[Re(bpy)(CO)_3(4\text{-}Etpy)]^+$ in both the ground and excited states. Table 5 lists the calculated frequencies for the three carbonyl modes in both the ground state and lowest MLCT state. Also given are force constants, reduced masses, and IR intensities for both the ground and excited states. Calculated energies for the vertical absorption (E(S→T)) and emission (E(T→S)) energies are shown below:

$$E(S\rightarrow T) = 19165\ cm^{-1}$$

$$E(T\rightarrow S) = 15374\ cm^{-1}$$

Table 6 lists calculated bond lengths and angles in the ground and excited states.

Discussion

For the two series *cis*-$[Os(pp)_2(CO)(L)]^{n+}$ and *fac*-$[Re(pp)(CO)_3(4\text{-}Etpy)]^+$, the magnitudes of the excited-state ν(CO) shifts, combined with the electrochemical and emission data, provide information about the electronic structure of the lowest-lying MLCT state(s). As noted in the Introduction, temperature-dependent lifetime measurements on related complexes reveal that the lowest-lying MLCT "state" is actually a manifold of three closely spaced states of common $d\pi-\pi^*$(pp) MLCT orbital parentage. These states are largely triplet in character and in rapid Boltzmann equilibrium.[10−12] The TRIR results reported here are presumably on a similar mixture of states in all cases.

Both series exhibit typical MLCT excited-state IR spectra.[2,5,7] As noted in the Introduction, the band energy of ν(CO) increases in the excited states. This has been interpreted as arising from partial oxidation at the metal which decreases $d\pi-\pi^*$(CO) back-bonding and increases CO multiple bond character.

Two ν(CO) bands appear in the ground-state spectra of *fac*-$[Re(pp)(CO)_3(4\text{-}Etpy)]^+$ consistent with C_{3v} symmetry, with the higher energy band arising from the A_1 normal mode and the broad, lower energy band from the E mode. The actual symmetry is C_s with overlapping A′(2) and A″ bands. In related molecules of lower local electronic symmetry, such as *fac*-$[Re(bpy)(CO)_3Cl]^+$, the two components of the "E" mode are resolved in the ground-state spectrum.

Three bands appear in the excited-state spectra consistent with the A′(1), A′(2), and A″ modes expected in C_s symmetry (see the Appendix). An analysis of these modes based on the procedures of Cotton and Kraihanzel[26] gives the local mode contributors illustrated in Figure 1 relative to the plane of the acceptor ligand. As shown in the Appendix, the correlation between the ground- and excited-state modes is $A_1 \rightarrow A'(1)$ and $E \rightarrow A'' + A'(2)$. On the basis of the results of our DFT calculations, the predicted energy ordering is A′(1) > A′(2) > A″, Table 5.

***cis*-[Os(pp)$_2$(CO)(L)]$^{n+}$.** In this series, variation in the ancillary ligand L from H^- to PPh_3 leads to an increase in the excited-to-ground-state MLCT energy gap, E_0, from 14000 to 19200 cm^{-1}, Table 1. The energies of the lowest π^* acceptor levels for bpy or phen as acceptor ligands are nearly the same.[27] The variation in the $Os^{III}(pp^{\bullet-})$ energy gap is a result of $d\pi$(Os)−L interactions, with electron donation from H^- stabilizing the excited state and $d\pi-\pi^*$ back-bonding to CH_3CN or PPh_3 stabilizing the ground state.

(26) Cotton, F. A.; Kraihanzel, C. S. *J. Am. Chem. Soc.* **1962**, *84*, 4432−4438.
(27) Kober, E. M.; Meyer, T. J. *Inorg. Chem.* **1985**, *24*, 106−108.

Table 3. Ground-State ($\bar{\nu}_{gs}$) and Excited-State ($\bar{\nu}_{es}$) Infrared Band Energies (± 2 cm^{-1}) and Shifts ($\Delta\bar{\nu} = \bar{\nu}_{es} - \bar{\nu}_{gs}$), Energy Gaps ($E_0$), and $E_{1/2}$ Values for *fac*-[Re(pp)(CO)$_3$(4-Etpy)]$^+$ in Acetonitrile at 298 K

	$\Delta\bar{\nu}$ (cm^{-1})			$\bar{\nu}_{gs}$ (cm^{-1})		$\bar{\nu}_{es}$ (cm^{-1})					
complex[a]	A″	A′(2)	A′(1)	E	A_1	A″	A′(2)	A′(1)	E_0[b] (cm^{-1})	$E_{1/2}(Re^{II/I})$[c] **(V)**	$E_{1/2}(bpy^{-/0})$[c] (V)
[Re(phen)(CO)$_3$(4-Etpy)]$^+$	31	80	26	1931	2036	1962	2011	2062	18300	1.83	−1.03
[Re(4,4′-(CH$_3$)$_2$bpy)(CO)$_3$(4-Etpy)]$^+$	37	81	33	1927	2034	1964	2008	2067	18700	1.78	−1.16
[Re(4,4′-(CH$_3$O)$_2$bpy)(CO)$_3$(4-Etpy)]$^+$	41	87	37	1921	2033	1962	2008	2070	18000	1.75	−1.19
[Re(bpy)(CO)$_3$(4-Etpy)]$^+$	44	83	39	1927	2035	1971	2010	2074	17900	1.74	−1.17
[Re(4,4′-(CO$_2$Et)$_2$bpy)(CO)$_3$(4-Etpy)]$^+$	45	88	54	1933	2038	1978	2023	2092	16200	1.89	−0.77

[a] As PF_6^- salts. [b] From Table 4. [c] Vs SSCE.

Table 4. Emission Spectral Fitting Parameters and $\Delta\bar{\nu}$ from Table 3 for *fac*-[Re(pp)(CO)$_3$(4-Etpy)]$^+$ in Acetonitrile at 298 K[a]

	$\Delta\bar{\nu}$ (cm^{-1})			E_0	E_{em}		$\Delta\bar{\nu}_{1/2}$
complex[b]	A″	A′(2)	A′(1)	(cm^{-1})	(cm^{-1})	S	(cm^{-1})
[Re(phen)(CO)$_3$(4-Etpy)]$^+$	31	80	26	18300	17900	1.4	2230
[Re(4,4′-(CH$_3$)$_2$bpy)(CO)$_3$(4-Etpy)]$^+$	37	81	33	18700	18500	1.4	2700
[Re(4,4′-(CH$_3$O)$_2$bpy)(CO)$_3$(4-Etpy)]$^+$	41	87	37	18000	17700	1.1	3100
[Re(bpy)(CO)$_3$(4-Etpy)]$^+$	44	83	39	17800	17500	1.1	3000
[Re(4,4′-(CO$_2$Et)$_2$bpy)(CO)$_3$(4-Etpy)]$^+$	45	88	54	16200	16000	1.0	2500

[a] $\hbar\omega$ was fixed at 1450 cm^{-1}. [b] As PF_6^- salts. [c] From Table 3.

Table 5. Calculated Parameters for the ν(CO) Vibrational Modes in *fac*-[Re(bpy)(CO)$_3$(4-Etpy)]$^+$ [a]

	$\bar{\nu}$ (cm^{-1})	μ (amu)	k (mdyn/Å)	I_{IR} (KM/mol)
		Ground State		
A′(1)	2120	13.28	35.15	843.2 (0.92)
A′(2)	2049	13.34	33.0	901.1 (0.98)
A″	2038	13.31	32.57	917.5 (1.00)
		^{3}MLCT		
A′(1)	2135	13.34	35.83	1312.1 (1.00)
A′(2)	2093	13.36	34.47	894.6 (0.68)
A″	2060	13.35	33.37	678.3 (0.52)

[a] The relative IR intensities are given parenthetically in the last column. μ and k are the reduced mass and force constant, respectively.

The spectroscopically derived energy gap is directly related to ΔG°_{ES} (the free energy of the excited state above the ground state) by $\Delta G^\circ_{ES} = E_0 + \lambda_{o,L}$. The quantity $\lambda_{o,L}$ is the sum of the solvent reorganizational energy (λ_o) and the reorganizational energy contributed by low-frequency modes treated classically.[17,28] For *cis*-[Os(phen)$_2$(CO)Cl]$^+$, for example, $E_0 = 14800$ cm^{-1} and $\lambda_{o,L} = 1800$ cm^{-1}, giving $\Delta G^\circ = 16600$ cm^{-1}. Since there is little variation in $\Delta\bar{\nu}_{1/2}$ in the Os series, (Table 2, 2020−2300 cm^{-1}), variations in E_0 are paralleled by variations in ΔG°_{ES}.

The ν(CO) stretch in the ground state acts as a "spectator" to changes in electronic structure at Os^{II} as the ancillary ligand L is varied. The increase in $\bar{\nu}_{gs}$ from 1911 to 1979 cm^{-1} from L = H^- to L = CH_3CN illustrates the effect of changing from the electron-donating hydride ligand to acetonitrile, which is a good back-bonding ligand for Os^{II}. The increase is caused by a combination of σ and π effects. Electron donation from H^- increases electron content at the metal and enhances dπ(Os^{II})−π^*(CO) back-bonding. This decreases C−O triple bonding and the energy of ν(CO). For L = CH_3CN competitive dπ(Os^{II})−π^*($NCCH_3$) back-bonding decreases dπ(Os^{II})−π^*(CO) back-bonding and increases ν(CO). The increase in $\bar{\nu}_{gs}$ parallels the increase in $E_{1/2}(Os^{III/II})$ (0.90−1.80 V vs SSCE in acetonitrile) and E_0 (14800 cm^{-1} for L = Cl^- to 18400 cm^{-1} for L = CH_3CN). This leads to the conclusion that the dominant orbital interaction in the ground-state energy gap correlation is the effect of L on dπ(Os).

Figure 4A shows plots of $\bar{\nu}_{gs}$ and $\bar{\nu}_{es}$ versus E_0. They reveal that variations in $\bar{\nu}_{es}$ with energy gap roughly parallel those in $\bar{\nu}_{gs}$. They are not exactly parallel. The difference between them, $\boldsymbol{\Delta}\bar{\nu} = \bar{\nu}_{es} - \bar{\nu}_{gs}$, decreases linearly from 76 cm^{-1} for L = H^- to 68 cm^{-1} for L = CH_3CN, Figure 4B. The PPh_3 complex does not fit well in either correlation (circled points in Figure 4A). This may be due to the steric effect of PPh_3 on dπ orbital mixing.

An orbital mixing scheme that provides a qualitative explanation for the variations in $\bar{\nu}_{gs}$ and E_0 with L is shown in the schematic energy level diagram in Scheme 1 for L = H^- and CH_3CN. As discussed above, a combination of σ and π effects leads to the dπ(Os^{II}) energy ordering, L = H^- > L = CH_3CN. This decreases $E_{1/2}(Os^{III/II})$ and the dπ(Os^{II})−π^*(bpy) energy gap for L = H^- compared to L = CH_3CN. It also decreases the dπ(Os^{II})−π^*(CO) energy gap, which enhances dπ(Os^{II})−π^*(CO) mixing.

The data in Figure 4A show that the increase in $\bar{\nu}_{gs}$ with E_0 (and the extent of dπ−π^*(CO) mixing) is nonlinear in E_0 as shown by the plot in Figure 4C. Excluding the point for L = PPh_3, there is an inverse−inverse relationship between $\bar{\nu}_{gs}$ and E_0. From the best fit straight line through the data, $\bar{\nu}_{gs}$ and E_0 are related by $\bar{\nu}_{gs} = \bar{\nu}_{gs,0}E_0/(E_0 + 0.58\bar{\nu}_{gs})$.

By extrapolation, $\bar{\nu}_{gs,0}$, the ν(CO) band energy in the limit of an infinite MLCT energy gap and no dπ(Os^{II})−π^*(CO) back-bonding, is 2111 ± 2 cm^{-1}.

Upon oxidation to Os^{III}, the dπ(Os) orbitals decrease in radial extension and the dπ(Os) energy levels are highly stabilized, which creates a large dπ(Os)−π^*(CO) energy gap. The resulting loss in Os−CO back-bonding is evident in the typical instability of Os^{III} complexes toward loss of CO. Consequently, in both Os^{III} and the Os^{III}(bpy$^{\bullet-}$) MLCT excited states, dπ(Os^{II})−π^*(CO) back-bonding is greatly decreased.

As shown in Figure 4, variations in $\bar{\nu}_{es}$ and $\bar{\nu}_{gs}$ with L and E_0 are nearly parallel. This suggests that variations in back-

(28) Chen, P.; Meyer, T. J. *Chem. Rev.* **1998**, *98*, 1439−1477.

Table 6. Bond Lengths (Å) and Angles (deg) in the B3LYP Approximation for the Ground State and Lowest MLCT Excited State of $[Re(bpy)(CO)_3(4\text{-Etpy})]^{+}$ [a]

	ground state	MLCT excited state		ground state	MLCT excited state
$R(Re-CO_{ax})$ (Å)	1.941	1.997	$\theta(Re-C-O)_{ax}$ (deg)	179.6	179.4
$R(Re-CO_{eq})$ (Å)	1.936	1.980	$\theta(Re-C-O)_{eq}$ (deg)	177.3	179.6
$R(CO_{ax})$ (Å)	1.156	1.146	$\theta(CO-Re-C-O)_{eq-eq}$ (deg)	90.5	86.8
$R(CO_{eq})$ (Å)	1.159	1.153	$\theta(CO-Re-C-O)_{eq-ax}$ (deg)	90.3, 90.9	91.4, 91.9
$R(Re-N_{bpy})$ (Å)	2.205	2.124			
$R(Re-N_{4-Etpy})$ (Å)	2.265	2.218			

[a] With the present basis set, the calculated R(CO) in free CO is 1.138 Å compared to the experimental value of 1.143 Å.[35]

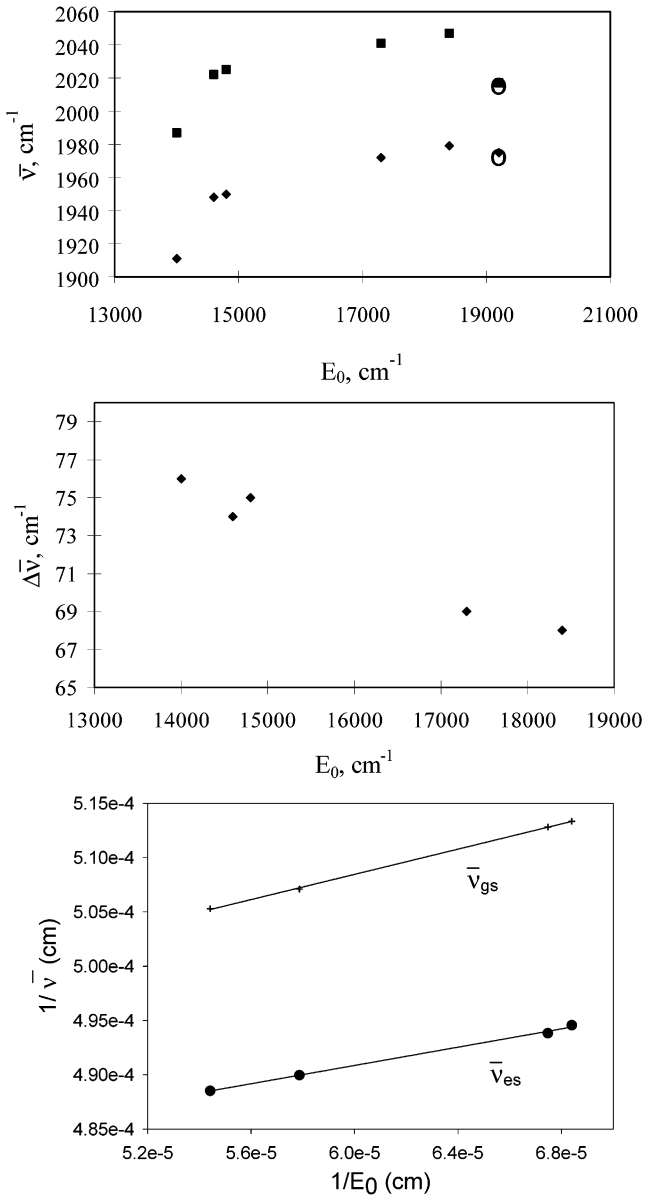

Figure 4. (A, top) $\bar{\nu}_{gs}$ (◆) and $\bar{\nu}_{es}$ (■) versus E_0 in acetonitrile at 298 K for *cis*-$[Os(pp)_2(CO)(L)]^{n+}$. (B, middle) $\Delta\bar{\nu}$ versus E_0 from Table 1. The circled points in (A) are for L = PPh_3 (see the text). This point is excluded in the correlation in (B). (C, bottom) Inverse−inverse plot of $1/\bar{\nu}_{gs}$ (+) and $1/\bar{\nu}_{es}$ (●) vs $1/E_0$ (PPh_3 has been excluded). Also shown are the linear fits to $1/\bar{\nu}_{gs} = \bar{\nu}_{gs,0} + a(1/E_0)$ and $1/\bar{\nu}_{es} = \bar{\nu}_{es,0} + a(1/E_0)$. The fits give $\bar{\nu}_{gs,0} = 2111 \pm 2$ cm^{-1} ($a = 0.58$) and $\bar{\nu}_{es,0} = 2148 \pm 4$ cm^{-1} ($a = 0.42$).

bonding with L also dominate in the excited state, but there are three additional electronic effects that may influence $\bar{\nu}_{es}$.

(1) σ(M−CO) Bond Polarization. In experiments on CO adsorbed to a zeolite in an applied electric field, the energy of ν(CO) was found to increase by 100 cm^{-1} per

Scheme 1

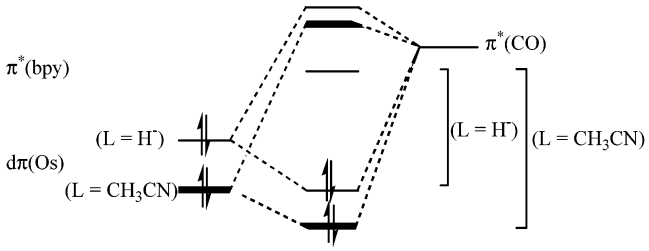

atomic unit of positive applied charge.[29,30] This so-called "vibrational Stark effect" is mimicked to a degree in the formation of the MLCT excited states, $Os^{III}(bpy^{\bullet-})$, where partial oxidation at the metal creates an internal electric field. At the orbital level, this leads to an increase in the dσ(Os) character in the Os−CO bond and electronic polarization toward the partly oxidized metal. The local electric fields can be significant. On the basis of variations in absorption band energies with solvent, the MLCT excited-state dipole moment in $[Ru^{III}(bpy^{\bullet-})(bpy)_2]^{2+*}$ has been estimated to be 14 ± 4 D.[31−33]

The magnitude of the vibrational Stark effect and its influence on $\bar{\nu}_{es}$ are expected to increase with E_0. The internal electric field created in the MLCT excited states increases with the energy gap. This occurs because there is less excited−ground-state mixing and increased charge-transfer character as E_0 increases. This increases the positive charge at Os and the negative charge at the bpy acceptor ligand.[17]

As shown by the inverse−inverse plot in Figure 4C, there is also an inverse−inverse relationship between $\bar{\nu}_{es}$ and E_0 with $\bar{\nu}_{es} = \bar{\nu}_{es,0}E_0/(E_0 + 0.42\bar{\nu}_{es,0})$.

$\bar{\nu}_{es,0}$, the magnitude of ν(CO) in the limit of complete charge transfer, is 2148 ± 4 cm^{-1}.

There is independent experimental evidence that charge-transfer character increases with E_0. One of the parameters derived from the emission spectral fitting procedure is S, the electron-vibrational coupling constant. It is related to the change in equilibrium displacement between the excited and ground states for the average coupled ν(bpy) mode, ΔQ_e, by $S \propto (\Delta Q_e)^2$.[16,17] S is a measure of the structural change at the acceptor ligand in the excited state. For bpy as the acceptor ligand, S increases from 1.2 for L = Cl^- with E_0 = 14800 cm^{-1} to 1.4 for L = CH_3CN with E_0 = 18400 cm^{-1}.

(29) Hush, N. S.; Reimers, J. R. *J. Phys. Chem.* **1995**, *99*, 15798−15805.
(30) Hush, N. S.; Williams, M. L. *J. Mol. Spectrosc.* **1974**, *50*, 349−368.
(31) Bates, W. D. Ph.D. Dissertation, University of North Carolina at Chapel Hill, Chapel Hill, NC, 1995.
(32) Kober, E. M.; Marshall, J. L.; Dressick, W. J.; Sullivan, B. P.; Caspar, J. V.; Meyer, T. J. *Inorg. Chem.* **1985**, *24*, 2755−2763.
(33) Kober, E. M.; Meyer, T. J. *Inorg. Chem.* **1982**, *21*, 3967−3977.

In an earlier study based on a more extensive series of Os^{II}(bpy) complexes, S was found to vary from 0.68 to 1.20 as E_0 increased from 13400 to 19200 cm^{-1}.[32]

(2) π^*(bpy$\bullet^-$)$-\pi^*$(CO) Mixing. The role of π^*(bpy$\bullet^-$)$-\pi^*$(CO) mixing will be discussed in the next section. It should be noted here that π^*(bpy$\bullet^-$)$-\pi^*$(CO) mixing increases the electron density in π^*(CO), which decreases $\bar{\nu}_{es}$. The extent of mixing increases with increasing charge-transfer character and contributes to the decrease in $\Delta\bar{\nu}$ with E_0 in Figure 4B.

(3) dπ(Os)$-\pi$(pp) Mixing. Another influence on the energy gap, $\bar{\nu}_{es}$, and $\Delta\bar{\nu}$ is dπ(Os)$-\pi$(pp) orbital mixing in the excited state. Promotion of the electron in the excited state, dπ^6(Os)π^*(bpy)^0 $\rightarrow$ dπ^5(Os)π^*(bpy)^1, creates a hole in the dπ orbitals. This provides a basis for dπ(Os)$-\pi$(pp) orbital mixing, which is the orbital basis for MLCT$-\pi\pi^*$ excited-state mixing. The extent of dπ(Os)$-\pi$(pp) mixing increases in the order L = CH_3CN > py > Cl^- > H^-, as the energy gap between the dπ(Os) and π(pp) levels decreases.

***fac*-[Re(pp)(CO)$_3$(4-Etpy)]$^+$.** In the *fac*-[Re(pp)(CO)$_3$(4-Etpy)]$^+$ series, the energy gap is varied by varying X in the 4,4′-X_2bpy acceptor ligand. All three ν(CO) bands shift to higher energy in the MLCT excited states, but to a different extent, with $\Delta\bar{\nu}$ largest for the A′(2) mode (Table 3). The overlapping E mode bands in the ground state are resolved into separate A′(2) and A″ bands in the excited states. Variations in band energies with X are small in the ground state, within experimental error for the highest energy band. There are variations in $\bar{\nu}_{es}$, but they are highly mode-specific. $\Delta\bar{\nu}$ varies 8 cm^{-1} for A′(2), 14 cm^{-1} for A″, and 28 cm^{-1} for A′(1).

Variations of $\bar{\nu}_{gs}$, $\bar{\nu}_{es}$, and $\Delta\bar{\nu}$ with the MLCT energy gap are illustrated in Figure 5. In contrast to the Os^{II} series in Figure 4A, ν_{es} *decreases* with E_0, at least for A′(1) and A″ (Figure 5B). The largest variation occurs for A′(1), with ν_{es} decreasing from 2092 cm^{-1} for X = CO_2Et (E_0 = 16200 cm^{-1}) to 2067 cm^{-1} for X = CH_3 (E_0 = 18700 cm^{-1}).

In this series, variations in the energy gap are caused by differences in the energies of the π^* acceptor orbital induced by the variations in X. Variations in $\Delta\bar{\nu}$ with E_0 occur almost solely in $\bar{\nu}_{es}$ (Figure 5C). $\bar{\nu}_{gs}$ is relatively unaffected by variations in X because these variations have only a small effect on the energy of dπ(Re^I) and on dπ(Re^I)$-\pi^*$(CO) back-bonding.

The general shift of $\bar{\nu}_{es}$ to higher energy compared to $\bar{\nu}_{gs}$ can be explained by loss of dπ(Re)$-\pi^*$(CO) back-bonding and σ(Re$-$CO) bond polarization in the Re^{II}(4,4′-X_2bpy$\bullet^-$) MLCT excited states. An additional electronic interaction must be invoked to explain the decrease in $\bar{\nu}_{es}$ with E_0.

A possible explanation is suggested in the energy level diagram in Scheme 2 for X = Me and CO_2Et. It is a schematic illustration of the mixing that occurs between the lowest π^*(4,4′-X_2bpy) level in the acceptor ligand and the in-plane π^*(CO) orbitals in the MLCT excited states. The relative orientations of the orbitals involved in the mixing can be surmised from Figure 1. π^*(4,4′-X_2bpy$\bullet^-$)$-\pi^*$(CO) mixing delocalizes the excited electron onto the CO ligands,

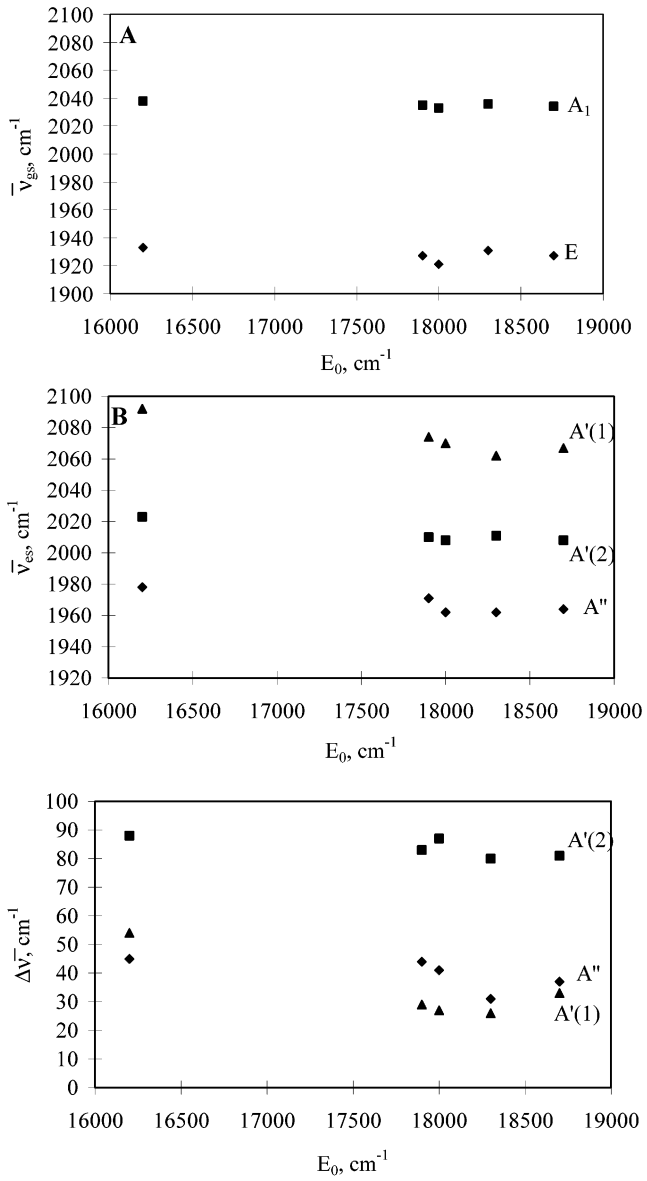

Figure 5. (A, top) $\bar{\nu}_{gs}$ versus E_0 in acetonitrile at 298 K for *fac*-[Re(pp)(CO)$_3$(4-Etpy)]$^+$ (A$_1$, ■, E, ◆). (B, middle) $\bar{\nu}_{es}$ versus E_0 in acetonitrile at 298 K for *fac*-[Re(pp)(CO)$_3$(4-Etpy)]$^+$ (A′(1), ▲; A″, ◆; A′(2), ■). (C, bottom) $\Delta\bar{\nu}$ versus E_0 (A′(1), ▲; A″, ◆; A′(2), ■). The data are from Table 1.

Scheme 2

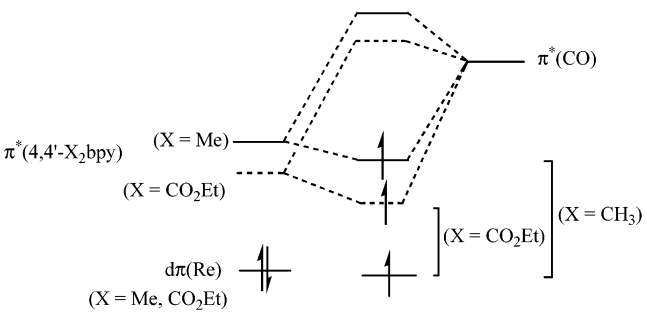

with the largest effect on the equatorial CO ligands. This decreases the CO bond order and $\bar{\nu}_{es}$. The effect is greater for X = CH_3 because the smaller π^*(4,4′-X_2bpy$\bullet^-$)$-\pi^*$(CO) energy gap enhances the degree of mixing.

A related effect has been observed in the ligand-based $\pi\pi^*$

excited states of $[Re(dppz)(CO)_3(PPh_3)]^+$ and $[Re(Me_2dppz)(CO)_3(4\text{-Etpy})]^+$ (dppz is dipyrido[3,2-*a*:2′,3′-*c*]phenazine; Me_2dppz is dimethyldipyrido[3,2-*a*:2′,3′-*c*]phenazine). In these excited states $\boldsymbol{\nu}$(CO) also shifts to slightly lower energy because of $\boldsymbol{\pi^*}$(dppz•$^-$)−$\boldsymbol{\pi^*}$(CO) mixing.[34]

The extent of $\pi^*(4,4'\text{-}X_2bpy^{\bullet-})-\pi^*(CO)$ mixing increases in the order X = CO_2Et < H < CH_3O < CH_3, as the energy of $\pi^*(4,4'\text{-}X_2bpy)$ increases and the $\pi^*(4,4'\text{-}X_2bpy)-\pi^*(CO)$ energy gap decreases. This provides a qualitative explanation for the decrease in $\bar{\nu}_{es}$ as the MLCT energy gap increases.

The results of the DFT calculations on the ground and lowest triplet states of $[Re(bpy)(CO)_3(4\text{-Etpy})]^+$ reinforce these conclusions and provide additional insights. For the ground state, the calculations predict the energy ordering of the carbonyl normal modes to be A′(1) > A′(2) > A″ with calculated frequencies of 2120, 2049, and 2038 cm^{-1}, respectively. These values compare to bands at 2035 cm^{-1} and the overlapping A′(2) and A″ bands at 1927 cm^{-1} found experimentally. The absolute frequencies in the DFT calculations are high, but the calculations do a reasonable job at predicting the separation between A_1 and the degenerate E modes (80 cm^{-1} calculated, 110 cm^{-1} observed).

The excited-state calculations show that the carbonyl band energies retain the same energy ordering in the excited state with all three shifted to higher energy. Again, the absolute excited-state energies are too high, but energy differences are comparable (30−40 cm^{-1} calculated, 50 cm^{-1} observed). The calculated excited-to-ground-state shifts are too small by ∼2. The vertical DFT calculated energy of absorption is 19165 cm^{-1}. The value calculated from the spectral fitting parameters and the relationship $\Delta G^\circ_{ES} = E_0 + S\hbar\omega + (\Delta\bar{\nu}_{1/2})^2/(16RT \ln 2)$ is 23400 cm^{-1}.

Once the excited state is formed, there is selective $\pi^*(4,4'\text{-}X_2bpy^{\bullet-})-\pi^*(CO)$ in-plane mixing. The π^*(CO) orbitals for the axial CO ligand are orthogonal to the plane and mix far less. The DFT calculations are consistent with this prediction. In the excited state they predict a decrease in the OC−Re−CO bond angle to 86.4° for the equatorial CO ligands compared to 90.5° in the ground state to maximize $\pi^*(4,4'\text{-}X_2bpy^{\bullet-})-\pi^*(CO)$ overlap. The increase in equatorial−axial bond angles from 90.3° and 90.9° in the ground state to 91.4° and 91.9° in the excited state can be attributed to enhanced electron−electron repulsion due to buildup of charge in the equatorial CO ligands.

In the A″ normal mode, the equatorial carbonyls move in an out-of-phase fashion. The DFT calculations predict that the OC−Re−CO bond angle should cause a decrease in A″ band intensity relative to that of A′(2). For A′(2) the equatorial carbonyls move in-phase, and the decrease in the OC−Re−CO angle causes a decrease in the magnitude of the transition dipole moment. The DFT calculations predict an A′(2):A″ intensity ratio of 1.3. This analysis provides an explanation for a common observation in the TRIR spectra of rhenium tricarbonyls. In the excited state, the intensity of the ∼2010 cm^{-1} band is always greater than that of the ∼1960−1970 cm^{-1} band and the ratio of intensities observed is consistent with the calculated A′(2):A″ ratio.

Experimentally, the magnitude of $\Delta\bar{\nu}$ and its variation with E_0 are mode-specific, with A′(2) varying from 80 to 88 cm^{-1}, A″ from 31 to 45 cm^{-1}, and A′(1) from 26 to 54 cm^{-1} (Figure 5C). This effect can also be explained by invoking $\pi^*(4,4'\text{-}X_2bpy^{\cdot-})-\pi^*(CO)$ mixing if the local mode compositions of the ν(CO) normal modes are taken into account. Local mode compositions are shown below, with equatorial (eq) referring to the in-plane CO ligands and axial (ax) to the perpendicular CO:[34]

$$A'(1) = 0.4717r_{ax}, 0.6235r_{eq}$$

$$A'(2) = 0.8828r_{ax}, 0.3335r_{eq}$$

$$A'' = 0.0r_{ax}, 0.7071r_{eq}$$

This analysis shows that the A′(1) and A″ modes have significant contributions from the equatorial CO ligands and they dominate $\pi^*(4,4'\text{-}X_2bpy^{\bullet-})-\pi^*(CO)$ mixing. This increases electron density in π^*(CO) and decreases the CO force constants and band energies. It also makes these modes more responsive to variations in X. For A′(2), there is a great deal of axial character. This mode is less influenced by $\pi^*(4,4'\text{-}X_2bpy^{\bullet-})-\pi^*(CO)$ mixing and in-plane delocalization. This explains the large value of $\Delta\bar{\nu}$ and the small variations with X. For A′(2), the magnitude of $\Delta\bar{\nu}$ is dictated largely by loss of $d\pi(Re)-\pi^*(CO)$ back-bonding, and σ(Re−CO) bond polarization in the excited states. $\pi^*(4,4'\text{-}X_2bpy^{\bullet-})-\pi^*(CO)$ mixing is relatively unimportant.

Conclusions

Variations in ν(CO) band energies in the ground and MLCT excited states in the series *cis*-$[Os(pp)_2(CO)(L)]^{n+}$ and *fac*-$[Re(pp)(CO)_3(4\text{-Etpy})]^+$ can be accounted for qualitatively by invoking a series of electronic interactions. Variations in $d\pi(M)-\pi^*(CO)$ back-bonding dominate in the ground state. In the excited states, there are three interactions: (1) loss of $d\pi(M)-\pi^*(CO)$ back-bonding and σ(M−CO) bond polarization, due to partial oxidation at the metal, (2) $\pi^*(4,4'\text{-}X_2bpy^{\bullet-})-\pi^*(CO)$ mixing, which provides an orbital basis for mixing $\pi^*(4,4'\text{-}X_2bpy^{\bullet-})$- and π^*(CO)-based MLCT excited states, and (3) $d\pi(M)-\pi(pp)$ mixing, which provides an orbital basis for mixing MLCT and $\pi\pi^*$ excited states. The results of the DFT calculations on *fac*-$[Re^I(bpy)(CO)_3(4\text{-Etpy})]^{+*}$ support the importance of $\pi^*(4,4'\text{-}X_2bpy^{\bullet-})-\pi^*(CO)$ mixing by the predicted excited-state structural changes. The DFT analysis also provides an explanation for the relative intensities of the A′(2) and A″ ν(CO) normal modes in the excited states, the large excited-to-ground-state shifts in A′(2), and the relative insensitivity of A′(2) to variations in X.

Acknowledgment. This work was performed in part at Los Alamos National Laboratory under the auspices of the U.S. Department of Energy and was supported by funds

(34) Gamelin, D. R.; George, M. W.; Glyn, P.; Grevels, F.-W.; Johnson, F. P. A.; Klotzbucher, W.; Morrison, S. L.; Russell, G.; Schaffner, K.; Turner, J. J. *Inorg. Chem.* **1994**, *33*, 3246.

(35) Huber, K. P.; Herzberg, G. P. *Constants of Diatomic Molecules*; Van Nostrand Reinhold: New York, 1970.

provided by the University of California for the conduct of discretionary research by Los Alamos to J.R.S. Work at the University of North Carolina was supported by the U.S. Department of Energy under Grant No. DE-FG02-96ER 14607 to T.J.M. We thank Professor Noel Hush and Roger Sullivan for insightful conversations and W. Stephen Aldridge and Joseph A. Treadway for assistance with emission spectral fitting.

Appendix

Symmetries of the Excited State *ν*(CO) Modes. Assuming C_{3v} symmetry in the ground state, there are three σ_v mirror planes. In the coordinate system below, with *y* and *z* in the plane of the paper, and the C_3 axis along *z*, only σ_{xz} lies on a symmetry axis. σ_{xz} is the only mirror plane retained in the excited state.

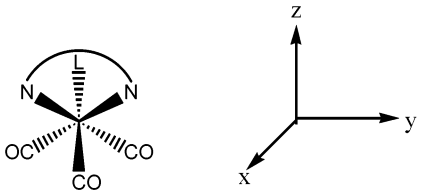

C_{3v}	E	$2C_3$	$3\sigma_v$	
A_1	1	1	1	*z*
A_2	1	1	-1	
E	2	-1	0	*(x,y)*

In the excited state, the symmetry is C_s. The only mirror plane in the excited state is σ_h, which is defined as σ_{xy} because there is no C_x rotation axis in C_s symmetry. σ_h in the excited state must correspond to σ_{xz} in the ground state, as it is the only mirror plane which is retained. This can be accomplished by an axis rotation:

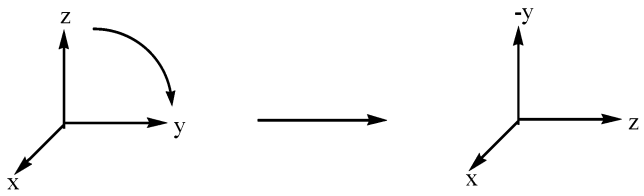

C_s	E	σ_h	
A'	1	1	*x,y*
A"	1	-1	*z*

In the new axis system, $\sigma_{xz} = \sigma_h$, but due to the rotation, *z* in C_{3v} becomes $-y$, and *xz* becomes *xy*. With this transformation, referring to the character table for C_s, A_1 in C_{3v} becomes $A'(y)$, and E becomes $A'(x)$ and $A''(z)$. On the basis of the ground-state analysis and the predicted effect of π^*(4,4′-X_2bpy)$-\pi^*$(CO) mixing in the excited state, the ground-to-excited-state correlations are $A_1 \rightarrow A'(y) = A'(1)$ and $E \rightarrow A'(x) + A''(z) = A'(2) + A''$.

IC020400I